JOURNAL OF MATERIALS SCIENCE 32 (1997) 3401–3406

DSC and TEM characterizations of thermal stability of an Al–Cu–Mg–Ag alloy

QIONG LI*, R. N. SHENOY
Analytical Services and Materials Inc., 107 Research Drive, Hampton VA 23666, USA

Assessment of long-term stability of an aluminium alloy exposed to elevated temperatures is important in the design of lightweight aerospace structures. The manner in which differential scanning calorimetry (DSC) and transmission electron microscopy (TEM) are used together in monitoring microstructural evolution, and thereby assess phase stabilities in an Al–5.1Cu–0.8 Mg–0.5 Ag–0.7 Mn–0.13 Zr (wt %) alloy, are described. DSC thermograms of the alloy, spanning room temperature to 400 °C, revealed the presence of two endotherms and an exotherm. TEM investigation has identified these thermal events to be associated with Ω, S′, and θ′ precipitates. Quantitative TEM was used to measure diameter, thickness, number density, and volume fraction of the precipitates in the alloy exposed at 135 °C for times as long as 3000 h. The quantitative TEM results are correlated with the DSC signatures relating to precipitation, dissolution, and coarsening reactions affecting the Ω, S′, and θ′ precipitates in the exposed alloy.

1. Introduction

Additions of small amounts of silver (~0.1 at %) to Al–Cu–Mg alloys effect significant enhancement of mechanical properties and thermal stability above 100 °C, through formation of the Ω phase [1, 2]. The Ω precipitates in silver containing Al–Cu–Mg alloys, with a composition close to Al_2Cu, nucleate and grow on matrix $\{1\,1\,1\}$ planes and exhibit a hexagonal plate morphology [3]. The Ω phase (unit cell parameters $a = 0.496$ nm, $b = 0.859$ nm, $c = 0.848$ nm; space group: Fmmm) is coherent with $\{1\,1\,1\}$ habit planes and has a misfit of -9.3% normal to the plane [4]. The Ω phase has also been described as a $\{1\,1\,1\}$ variant of the equilibrium θ (Al_2Cu) phase, with a slightly lower solvus temperature [5]. The dominance of either Ω or θ′ (Al_2Cu) formation is dictated by the Cu/Mg ratio in the alloy [6]. While a relatively low value of the ratio (~6) favours Ω, a high value (~10) favours θ′ [6, 7]. In addition, S′ (Al_2CuMg) and a small amount of S ($Al_5Cu_6Mg_2$) may also be noticed [8]. Relative stabilities of Ω and θ′ are also affected by coldwork prior to ageing [9]. Coldwork undermines Ω precipitation, while at the same time favouring θ′ formation. Thermal stability of the Ω phase in Al–Cu–Mg–Ag alloys with relatively high Cu/Mg ratios (~13–14), and aged at high temperatures (200–300 °C) was reported recently by Ringer *et al.* [10].

Based on the beneficial effects of silver in Al–Cu–Mg alloys, Alcoa has recently designed an Al–5.1Cu–0.8Mg–0.5Ag–0.7Mn–0.13Zr (wt %) alloy to be a candidate high-temperature material. Applications envisage long-term thermal exposure (several tens of thousands of hours) at temperatures as high as ~135 °C. The long-term exposure to which this alloy may be subjected can significantly alter the relative distributions of Ω, S′, and θ′ phases, and hence affect the thermal stability of the alloy. A comprehensive identification of phase transitions in the range room temperature–550 °C has been reported for the alloy in a companion study [11]. The present investigation purports to evaluate the long-term thermal stability of the alloy exposed at 107 and 135 °C for times as long as 3000 h, using DSC and TEM analyses.

2. Experimental procedure

The Al–5.1Cu–0.8Mg–0.5Ag–0.7Mn–0.13Zr (wt %) alloy, produced by Alcoa in the form of 2.3 mm thick sheet, was heat treated to a commercial T8 temper (5% stretch after solution treatment, followed by ageing at 160 °C for 16 h). Alloy sheets in the T8 temper were further exposed in air for times up to 3000 h each at 107 and 135 °C.

DSC: thermograms spanning room temperature–400 °C were obtained for the T8 and the variously exposed samples (DSC specimens 3.5 mm × 3.5 mm, 2.3 mm thick and weight of ~80 mg) were obtained in flowing dry nitrogen, using a TA Instruments 2910 DSC apparatus. A pure aluminum disc of approximately the same mass as a DSC specimen, was used as the reference.

Present address: Reynolds Metals Company, P.O. Box 27003, Fourth and Canal Streets, Richmond, VA 23236, USA.

0022–2461

TEM: a Philips EM 420 operating at 120 kV and equipped with a Kevex energy dispersive analyser, was used for microstructural characterization. TEM foils were prepared by electrolytic jet polishing, with a 70% methanol +30% HNO_3 bath at $-30\,^{\circ}C$ and 12 V.

Length, $L(\Omega)$, $L(S')$, and thickness, $t(\Omega)$ $t(S')$, measurements of the Ω and S′ phases (approximately 200 precipitates each) were made in the $\langle 1\,1\,2\rangle_{Al}$ dark-field (DF) images, because the precipitates are edge-on in this orientation. Calibrated values at nominal TEM magnifications of $\times 86\,000$ and $\times 300\,000$ were employed for measurements of L and t, respectively. The number density of precipitate per unit volume, N_V, was computed from a formula given by Hilliard [12].

$$N_V = 1/t_0[P_A - P_L/2t_0 + P_A P_P + (\pi P_L^2/16] \quad (1)$$

where t_0 is the foil thickness (estimated to be in the range of 90–100 nm), P_A the area point count, P_L the line intercept count, and P_P the point count. Volume fractions V_f (Ω) and V_f (S′), of Ω and S′, respectively, were computed as follows. V_f is the volume of one precipitate × number of precipitate variants × N_V for one precipitate variant. The number of precipitate varaints for Ω and S′, are respectively, 4 and 12. A hexagonal plate morphology for Ω, and a cylindrical shape for S′ were assumed in the computations.

3. Results and discussion

The processes occurring during the course of a thermal exposure may be identified as: precipitation of additional volume fractions of precipitates through fresh nucleation or growth of existing precipitates; progressive dissolution of precipitates; on-going coarsening of precipitates; and precipitation of new phases. Some or all of these processes may run concurrently at various time periods within an exposure. In the present study, these processes are sought to be monitored in post-exposure samples using the DSC and TEM techniques. It was recognized at the outset that thermal events in a DSC thermogram that are critical to the alloy stability *vis-à-vis* Ω, S′, and θ′ precipitate morphologies, occur mostly in the room temperature–300 °C temperature range. On the other hand, the various thermal events in the 300–550 °C range merely aid a general understanding of the microstructural evolution at higher temperatures [11]. With this in mind, DSC scans in the present study span only a limited range of room temperature–400 °C. The rationale for selection of 107 and 135 °C as the exposure temperatures is as follows. Close to 107 °C is a temperature that corresponds to maximal aerodynamic heating in certain applications [13]. Exposures at 135 °C, which is midway between 107 °C and the T8 ageing temperature of 163 °C, are expected to yield data relating to an accelerated degradation of alloy stability. While the DSC data were gathered for both 107 and 135 °C exposures, the TEM analysis of precipitate morphologies was done for only the 135 °C exposures.

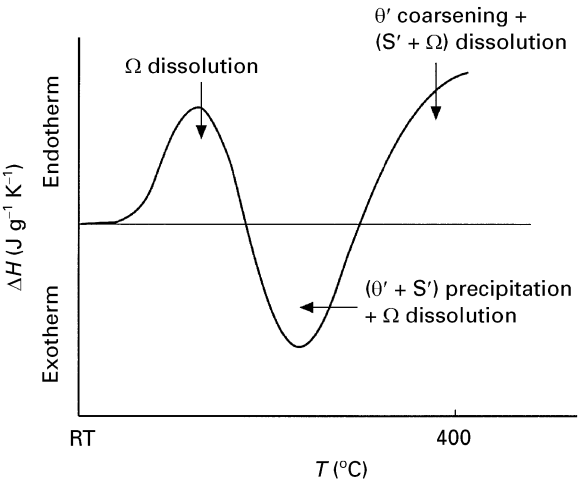

Figure 1 Schematic representation of the DSC thermogram for the T8 condition.

3.1. DSC

Fig. 1 is a schematic representation of a typical DSC thermogram for the T8 condition. The two endotherms and the exotherm, occurring in the room temperature–400 °C range are identified therein [11]. The lower temperature endotherm relates dominantly to the dissolution of Ω. However, near the apparent end of this endotherm, precipitation of both S′ and θ′ is initiated, thereby resulting in a strong exotherm. Embedded also in this exotherm is a heat effect due to an on-going dissolution of residual Ω. The higher temperature endotherm accounts for dissolution of S′, coarsening of θ′, and dissolution of residual Ω. Because more than one process characterizes both the endotherm and the exotherm, these two thermal events are therefore not ideal candidates for a Johnson–Mehl–Avrami (JMA) type kinetics analysis to be performed on them. Besides, deconvolution of individual endothermic and exothermic heat effects was not attempted in the present study. Nevertheless, meaningful information that complements the TEM characterization of precipitate evolution in the alloy, can be gleaned from such a thermogram. For example, the area under the curve, A_{DSC}, peak temperature, T_P, full-width at half-maximum, FWHM, in a dissolution/precipitation peak are relatable to volume fraction, average precipitate size, and precipitate-size distribution, respectively [14].

Fig. 2 is a compilation of thermograms for the T8, and the variously exposed conditions. Values of A_{DSC} and T_P of the Ω dissolution endotherms, gleaned from Fig. 2 are presented in Fig. 3. The following observations and inferences may be made with reference to Figs 2 and 3.

(i) Judging from the A_{DSC} of the Ω dissolution endotherm, the 1000 and 3000 h exposures at 107 °C, and the 1000 h exposure at 135 °C, account for a nearly 55% increase in additional precipitation. This implies that the as-received T8 condition has extra supersaturation which is relieved during these exposures.

(ii) The (θ′ + S′) precipitation exotherms for the 107 °C exposures are essentially the same for both 1000 and 3000 h. This suggests that the 107 °C

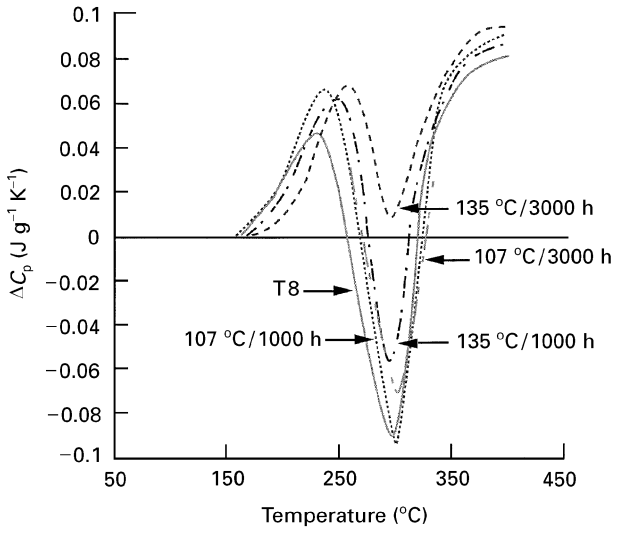

Figure 2 Differential heat capacity of the Al–Cu–Mg–Ag alloy for various thermal exposures. Scanning rate = 20 °C min^{-1}.

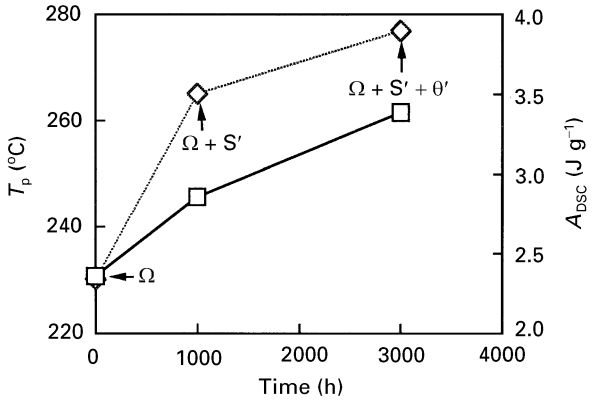

Figure 3 (□) T_P and (◇) A_{DSC} of the dissolution endotherm for the 135 °C exposures as a function of exposure time.

exposures yield microstructures which have very nearly constant volume fractions for S′ and θ′ phases. In contrast, the corresponding exotherm for the 135 °C/1000 h exposure has a smaller A_{DSC}. Also, for the 135 °C/3000 h exposure, the (θ′ + S′) precipitation exotherm has apparently disappeared. The smaller A_{DSC} for this exotherm or its disappearance in a thermogram, implies a corresponding increase in the volume fractions of θ′ and S′ in the microstructures for the 135 °C exposures. Conversely, during a DSC scan, part of this θ′ + S′ dissolves and contributes an additional endothermic heat into the A_{DSC} of the ostensible Ω dissolution endotherm.

(iii) Increases in T_P are relatable to significant increases in precipitate size brought about either by growth (precipitate lengthening) or coarsening (precipitate thickening). While growth involves increase in volume fraction; coarsening may accompany increase/decrease/constancy of volume fraction. Although, in general, it is not possible a priori to assign T_P solely to either L or t of a precipitate, it is nevertheless meaningful to regard T_P as being a measure of average particle size. In light of this DSC-related observation, a definitive corroboration must be sought from the TEM characterization of precipitates.

3.2. TEM

The strengthening precipitates involved in the exposure-related modifications of the alloy microstructure are Ω, S′, and θ′. Fig. 4 shows DF images of the precipitates for the T8 and 1000 and 3000 h exposures at 135 °C. Precipitate size, morphology, number density, and volume fraction can be quantified using stereological procedures. Only the Ω and S′ phases were subjected to a quantitative analysis.

Fig. 5 is a plot of precipitate-size variation with exposure time at 135 °C for the θ′ and S′ phases. The corresponding aspect ratio (L/t) variations are plotted in Fig. 6. The following observations may be made from Figs 5 and 6. (i) L increases in the 0–1000 h duration, for both Ω and S′, the increase being steeper for Ω than for S′. Beyond 1000 h, L decreases for both the precipitates. In contrast, t increases monotonically over the entire 0–3000 h duration for both Ω and S′, resulting in similar variations for the L/t ratio with

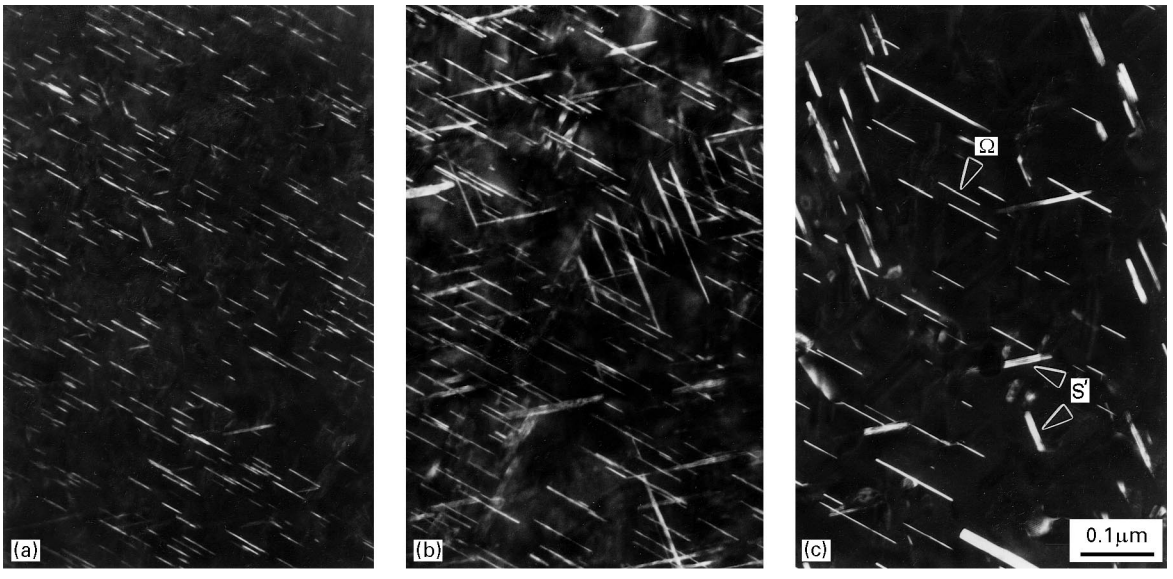

Figure 4 $\langle 1\,1\,2\rangle_{Al}$ DF images: (a) T8, dominantly Ω; (b) 135 °C/1000 h, Ω + S′; (c) 135 °C/3000 h, coarsened Ω + S′.

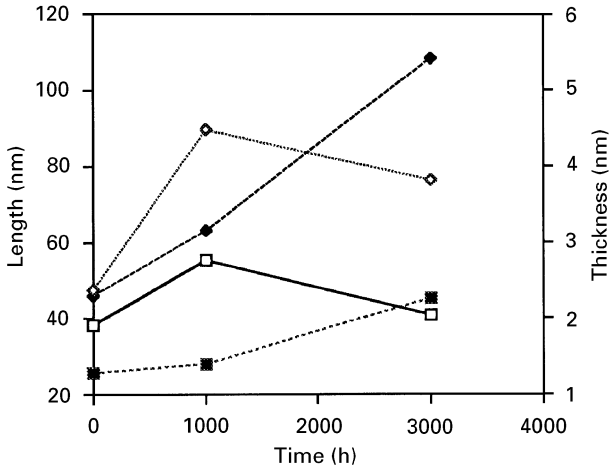

Figure 5 Precipitate size ((□, ◇) L and (■, ◆) t) as a function of exposure time at 135 °C: (□, ■) Ω, (◇, ◆) S′.

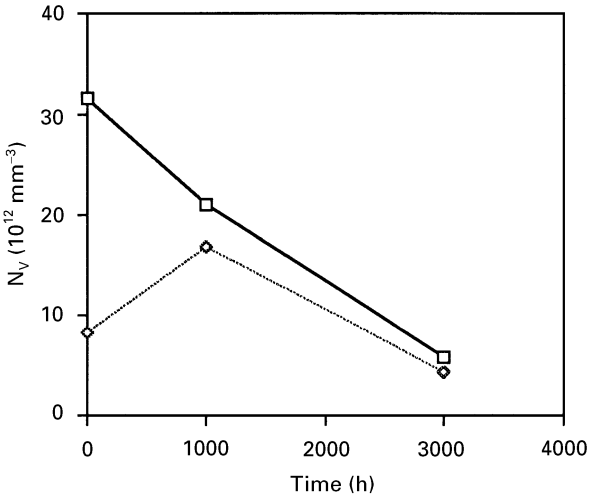

Figure 7 (□) N_V (Ω) and (◇) N_V(S′) as a function of exposure time at 135 °C.

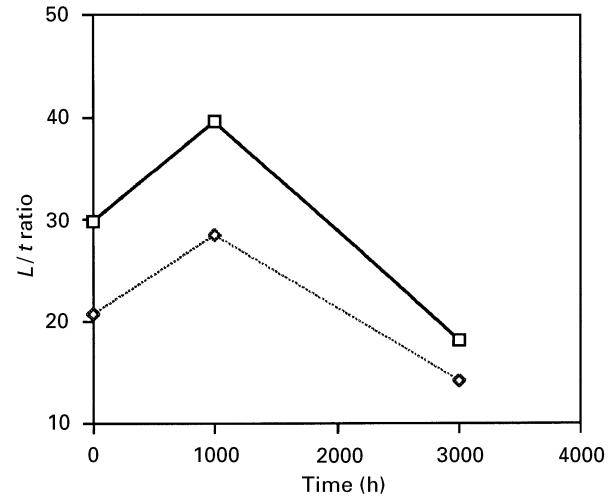

Figure 6 L/t ratio of the precipitates as a function of exposure time at 135 °C: (□) Ω, (◇) S′.

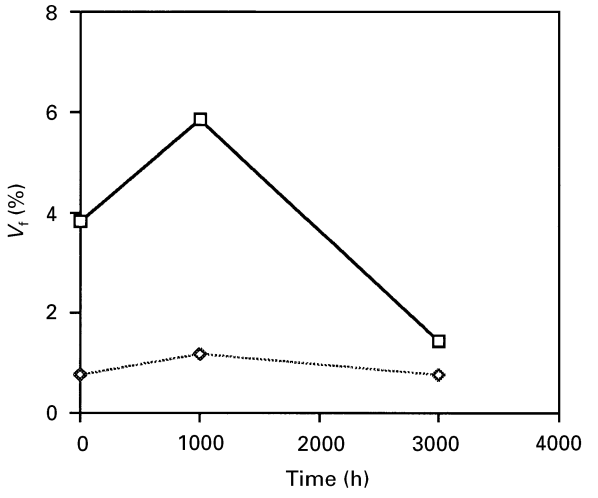

Figure 8 (□) V_f(Ω) and (◇) V_f(S′) as a function of exposure time at 135 °C.

exposure as for L. (ii) Increases in T_P (see Fig. 3) correlate well with increases in t for the precipitates.

The number density, N_V, of the Ω and S′ precipitates for the 135 °C exposures, are shown in Fig. 7. N_V(Ω) decreases monotonically from an initial value of 32×10^{12} mm^{-3} (in the T8 condition) to 5.8×10^{12} mm^{-3} by the end of 3000 h. N_V(S′), on the other hand, increases from an initial value of 8.3×10^{12} mm^{-3} to 16.8×10^{12} mm^{-3} at the end of 1000 h; thereafter, it decreases to 4.3×10^{12} mm^{-3} at the end of 3000 h.

Volume fractions, V_f(Ω) and V_f(S′) are shown in Fig. 8. V_f(Ω) increases from an initial value of 3.8% (in the T8 condition) to 5.9% by the end of 1000 h; thereafter it decreases steeply to ~1.4% at the end of 3000 h. V_f(S′) increases from an initial value of 0.16% to 1.2% for the 1000 h exposure, and decreases gradually to ~0.7% for the 3000 h exposure.

Based on the TEM results presented above, the following observations and inferences may be made with regard to precipitate evolution in the 135 °C exposures.

3.2.1. 1000 h

(i) The exposure results in additional precipitation, implying the T8 condition has significant level of supersaturation to begin with (see V_f(Ω) and V_f(S′) variations in Fig. 8).

(ii) The additional precipitation manifests dominantly in terms of the growth of Ω (see t(Ω) variation in Fig. 5).

(iii) Increases in L(S′) and N_V(S′), albeit mild (see Figs 5 and 7), imply that V_f(S′) increases through both precipitate growth, and fresh nucleation.

(iv) The decrease in N_V(Ω), despite the increases in L(Ω) and V_f(Ω), suggests that the Ω phase also experiences coarsening during the exposure.

3.2.2. 3000 h

(i) The large reduction in V_f(Ω), through dissolution in the matrix, indicates that the Ω phase is unstable in an extended exposure application. Accompanying this, is also a substantial coarsening of the phase, as suggested by steep decreases in N_V(Ω) and the aspect

ratio. Appreciable increase in T_P of the Ω dissolution endotherm (see Fig. 3), independently attests to the precipitate coarsening effect of the exposures.

(ii) The S′ phase is subjected primarily to coarsening, although a mild reduction in V_f(S′) is also experienced.

(iii) The TEM results show that the sum of $V_f(\Omega)$ and V_f(S′) is ∼2.5% for the 3000 h exposure, as opposed to ∼7% for the 1000 h exposure. In contrast to this, Fig. 3 shows that A_{DSC} (3000 h) > A_{DSC} (1000 h), for the ostensible Ω dissolution endotherm. Correspondingly, the θ′ + S′ exotherm (see Fig. 2) has apparently disappeared for the 3000 h exposure, while it is still prominent for the 1000 h exposure. As has been explained in the DSC section above, loss of the (θ′ + S′) exotherm implies the presence of copious amounts of θ′ in the 3000 h exposure microstructure. The reduction in $V_f(\Omega)$ through dissolution, then, must account for the increased presence of θ′. The $\langle 0\,0\,1\rangle_{Al}$ DF image in Fig. 9, indicating a strong presence of θ′, shows this to be indeed true.

3.3. Overall view of the Ω and θ′ evolution

The Al–5.1Cu–0.8Mg–0.5Ag–0.7Mn–0.13Zr (wt %) was designed, with the aim of producing Ω as the dominant strengthening precipitate after ageing at 163 °C for 16 h during a commercial T8 treatment. The TEM data in the present study support this premise. Once the alloy in the T8 condition is exposed to 135 °C for durations as long as 3000 h, however, thermal stability of the Ω phase is called into question. Both DSC and TEM results indicate that the 135 °C exposures cause copious precipitation of θ′, at the expense of Ω. For the 107 °C exposures, in contrast, the DSC thermograms (see Fig. 2) indicate that θ′ precipitation does not occur appreciably even at the end of the 3000 h. These ideas may be incorporated into a schematic time–temperature–transformation (TTT) diagram shown in Fig. 10. The temperatures of phase stability for Ω and θ′ shown therein are from the room temperature–550 °C DSC thermogram for the alloy [11]. The T8 ageing temperature of 163 °C, and the exposure temperatures of 107 and 135 °C, are also indicated. In such a plot, the relative positions of the Ω and the θ′ formation curves are expected to change significantly as a function the Cu/Mg ratio in the alloy [6, 7]. This means that when the Cu/Mg ratio is high (>10), formation of θ′ is favoured rather than Ω. The above TTT diagram also helps make a qualitative selection of exposure temperatures and times, in obtaining a Ω microstructure without θ′. From an applications point of view, the lack of thermal stability for Ω during an extended exposure at the intended service temperature would be undesirable. Ringer *et al.*'s [10] work suggests that the stability of Ω might be easy to ensure at ageing temperatures below 200 °C. The present study, however, indicates that for the composition considered, significant modifications to Ω are wrought by a 3000 h exposure even at 135 °C. One factor possibly contributing to the relative instability of Ω in the present alloy, is the 6% deformation to which the alloy was subjected during a commercial

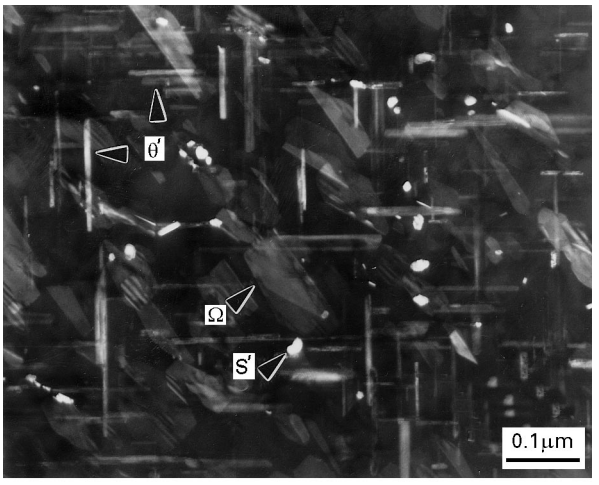

Figure 9 $\langle 1\,0\,0\rangle_{Al}$ DF image for the 135 °C/3000 h exposure, showing θ′ precipitates.

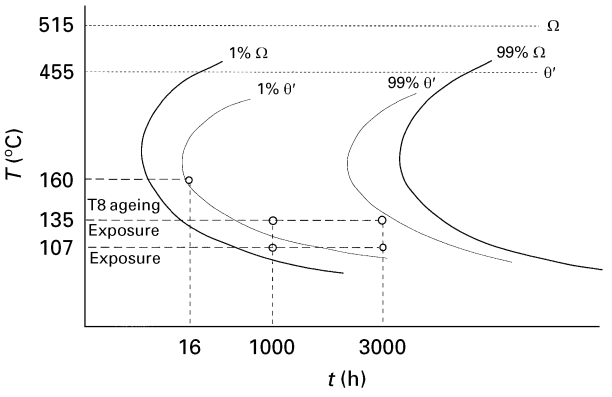

Figure 10 Schematic TTT diagram of Ω and θ′ formation in the Al–Cu–Mg–Ag alloy.

T8 treatment. That θ′ precipitation occurs at the expense of Ω in Al–Cu–Mg–Ag alloys when these alloys are cold worked prior to ageing, was reported recently [9]. In the light of this observation, it may be appropriate to assess long-term stability of Ω, in alloys that have not been cold worked subsequent to quenching from the solution heat-treatment temperature.

4. Conclusions

DSC and TEM characterizations of the Al–5.1Cu–0.8Mg–0.5Ag–0.7Mn–0.13Zr (wt %) alloy, subjected to long-term exposures indicate the following points.

1. The initial microstructure in the unexposed T8 condition is dominantly Ω. The T8 condition has substantial supersaturation, however. During the 1000 h exposures at 107 and 135 °C, this supersaturation is relieved through precipitation of additional Ω (major phase) and S′ (minor phase).

2. The thermal stability of Ω is undermined by a 135 °C/3000 h exposure, which results in a drastic reduction in volume fraction of Ω through dissolution and appreciable precipitation of θ′ in the microstructure. In the process, the volume fraction of S′ which is relatively low, remains substantially unaltered. In contrast, the 107 °C/3000 h exposure yields a microstructure

without loss of Ω (as indicated by near constancy of the A_{DSC} for the S′ + θ′ exotherm).

3. In relation to morphological changes in Ω and S′, it is the growth process that distinguishes the early part of the exposures (the initial 1000 h). During the latter part of the exposures (~1000–3000 h), however, it is the particle coarsening that predominates.

Acknowledgements

The work was performed in the Materials Division at NASA LaRC under Contract NAS1-19708. Constructive suggestions by Dr S. J. Hales, Analytical Services and Materials Inc, Hampton, VA, are gratefully acknowledged. The authors thank Messrs R. K. Bird, D. M. Royster and D. L. Dicus, NASA LaRC, for their encouragement.

References

1. I. J. POLMEAR, *Trans. Metall. Soc. AIME* **230** (1964) 1331.
2. *Idem*, *Metall. Trans.* **19A** (1988) 1027.
3. B. C. MUDDLE and I. J. POLMEAR, *Acta Metall. Mater.* **24** (1989) 777.
4. K. M. KNOWLES and W. M. STOBBS, *Acta. Crystallogr* **B44** (1988) 207.
5. Y. C. CHANG and J. M. HOWE, *Metall. Trans.* **24A** (1993) 1461.
6. V. D. SCOTT, S. KERRY and R. L. TRUMPER, *Mater. Sci. Technol.* **3** (1987) 827.
7. R. N. SHENOY and QIONG LI, manuscript in preparation.
8. R. SCHUELLER, A. K. SACHDEV and F. E. WAWNER, *Scripta Metall.* **27** (1992) 1289.
9. S. P. RINGER, B. C. MUDDLE and I. J. POLMEAR, *Metall Trans.* **26A** (1995) 1659.
10. S. P. RINGER, W. YEUNG, B. C. MUDDLE and I. J. POLMEAR, *Acta Metall. Mater.* **42** (1994) 1715.
11. QIONG LI and R. N. SHENOY, sent for publication.
12. J. E. HILLIARD, *Trans. Metall. Soc. AIME* **224** (1962) 906.
13. E. A. STARKE Jr, NASA Contractor Report 4517, Grant NAG1-745 (1993)
14. R. N. SHENOY and J.M. HOWE, *Scripta Metall. Mater.* **30** (1995) 651.

Received 24 June
and accepted 23 October 1996